Published by :
http://www.ijert.org

International Journal of Engineering Research & Technology (IJERT)
ISSN: 2278-0181
Vol. 11 Issue 04, April-2022

Modelling and Inverse Kinematics of Tendon Driven Continuum Robots using Cascade Correlation

Ashok Madan
Mechanical Engineering Department
Delhi Technological University
New Delhi, India

Shaswat Garg
Mechanical Engineering Department
Delhi Technological University
New Delhi, India

Satwik Dudeja
Mechanical Engineering Department
Delhi Technological University
New Delhi, India

***Abstract*— Inverse kinematics is among the most important challenges in robotics, since it is required to map the design space onto the joint space in order to permit smooth motion throughout any task. Inverse Kinematics is difficult to master because of the non-linearities and kinematic redundancy seen in continuum robots. We offer a static model for a tendon-driven continuum robot in this study, which is based on Cosserat string theory and rod theory. For inverse kinematics, we suggest using a neural network based on cascade correlation. Using 20,000 established training data, Cascade Correlation model reaches RMSE of 1.34 and 1.45 in training and testing. Comparative study is done by replicating models from previous literature, validating the accuracy of our proposed model.**

Keywords – Inverse Kinematics, Cascade Correlation, Continuum Robots, Tendon Driven Robots

I. INTRODUCTION

Since the last decade, continuum robots [1] seem to be a prominent problem in the context of robotics. For the researchers, nature has been a great source of inspiration. The remarkable mobility, manipulation, and dexterity skills of elephant trunks [2], snakes [3], and octopuses [4] in an unpredictable and chaotic environment have prompted researchers to construct continuum robots. A continuum robot is a robot with limitless degrees of freedom that bends continuously. In comparison to traditional robots, continuum machines can perform in complicated obstacle fields with relative ease due to their innate agility. They are commonly utilized for surgical operations [5] and disaster response in collapsed structures [6] due to their compliance. Pneumatic actuators [7], concentric tubes [8], tendon driven mechanisms [10], and shape memory alloys [9] can all be used to control continuum robots.

The kinematics of continuum robots is a fascinating and difficult topic to solve. Kinematics may be broken down into two types of mappings. From actuator or joint space, to configuration space is the first step. Aside from configuration space, there is task space, which describes the position and direction of the backbone. Two common strategies for tackling the problem are model-based [11] and machine learning [12]. Low fidelity lumped parameter models and high fidelity distributed parameter models are the two types of continuous robot modelling efforts [13]. External loadings like gravity cause variations in curvature over the length of the robot, which low-fidelity models disregard. To tackle kinematics problems, Jones B. et al. [14] designed a DH parameter representation. The kinematics of the robot were approximated as a set of stiff links connected by revolute and prismatic joints. To develop the kinematic equations, Wang He. et al. [15] suggested an analytical technique based on the Euler-Bernoulli beam. Arc geometry was utilized by Li M. et al. [16] to establish the kinematic relationship across the configuration space and the task space. The performance of lumped parameter models in real time is outstanding, but accuracy suffers. As a result, distributed parameter high fidelity models are employed to simulate an arbitrary form of a continuum robot. Jones B. et al. [17] proposed utilizing Cosserat rod theory to compute the form of a continuum robot. Rucker D. et al. [18] built on prior research by taking into account attachment point force, and distributed wrench tendon applications on the backbone. S. Song et al. [19] suggested a reconstruction approach based on a third-order Bezier curve for positional and directional data acquired from electromagnetic sensors positioned on the flexible robot's distal end. To develop the kinematics of a continuum robot, Ding J. et al. [20] introduced a pseudo rigid body model of beam.

Despite their excellent accuracy, distributed parameter models are computationally costly to solve. As a result, machine learning algorithms are employed since they are very accurate and can perform in real time once learned. Multilayer perceptron was utilized by Kuntz A. et al. [21] to anticipate the form of a 3-tube concentric tube robot. Using RBF, MLP, SVR, and CANFIS, Loutfi I. et al [22] calculated the forward kinematics of Compact Bionic Handling Assistant. A backpropagation neural network was used by Shahabi E. et al. [23] to train the inverse kinematics of a dual backbone robot. The dataset was created using the PRBM 3R model. G. Wu et al. [24] used RBF, MLP, and a combination of Genetic algorithm and MLP to study the kinematics of a parallel continuum robot. Lai et al. [25] used neural networks to address the problem for a dual segment continuum robot. DH Parameter Formulation was used to create the dataset. Shen W. et al. [26] used Gaussian Process Regression to tackle the forward kinematics problem of a Tendon-driven continuum robot. Inverse kinematics of a tendon-driven serpentine robot have also been devised using algorithms such as KNNR and Extreme learning machine

International Journal of Engineering Research & Technology (IJERT)
ISSN: 2278-0181
Vol. 11 Issue 04, April-2022

[27]. Thuruthel et al. [28] developed an MLP model to deal with several solution problems in inverse kinematics utilizing diverse mappings across configuration and task space.

Many existing learning-based kinematic solutions for continuum robots, on the other hand, have a large degree of inaccuracy, making them unsuitable for application in contexts such as surgical operations, where precision is critical. As a result, we concentrate on employing invertible neural networks to solve the problem. The method is evaluated on a Cosserat Rod theory-based Tendon-driven continuum robot with DOFs.

The following is how the rest of the paper is organised: The design of the Tendon-driven continuum robot is presented in Section II. The forward kinematic modelling study utilising Cosserat Rod theory is presented in Section III. In Section IV, a cascade correlation network model is used to train the robot's inverse kinematics. The results of the suggested integrated accuracy enhancement approach are presented in Section V to validate its efficacy. The conclusion of this study is presented in Section VI.

II. MODELLING OF CONTINUUM ROBOT

The Cosserat model introduced in [29] is used to represent the kinematics of the continuum robot. Both the tendon attachment points force and the distributional wrench the tendon exerts along the length of the backbone are taken into account in the aforementioned model. The backbone is defined by a p(s) center-line curve and R orientation (s). Therefore, the homogenous rigid body transformation is given by –

$$g(s) = \begin{bmatrix} R(s) & p(s) \\ 0 & 0 \end{bmatrix}$$

Given the linear and angular rates of change of $g(s)$ as $v(s)$ and $u(s)$. Thus, the evolution of $g(s)$ along s is defined as –

$$\dot{R}(s) = R(s)\hat{u}(s)$$
$$\dot{p}(s) = R(s)v(s)$$

The equations of static equilibrium of an arbitrary section of rod are given by [30] –

$$\dot{n}(s) + f(s) = 0$$
$$\dot{m}(s) + \dot{p}(s) \times n(s) + l(s) = 0$$
$$n(s) = R(s)K_{se}(s)(v(s) - v^*(s))$$
$$m(s) = R(s)K_{bt}(s)(u(s) - u^*(s))$$

Where, the applied force distribution per unit of s is given by f the applied moment distribution per unit of s is l. n and m denote the internal force and moment vectors respectively. The kinematic variables in undeformed reference configuration are given by v^* and u^*. K_{se} is the stiffness matrix for shear and extension and K_{bt} is the matrix for bending and torsion. Now combining the rod model with the Cosserat model for extensible strings to describe the tendons we get –

$$f = f_e + f_t$$
$$l = l_e + l_t$$

Where, f_e and l_e are truly external distribution loads and f_t and l_t are distribution loads due to tendon tension. The tendon location in the body coordinate frame is given by –

$$r_i(s) = [x_i(s) \quad y_i(s) \quad 0]^T$$

The parametric space curve defining the tendon path in deformed state is given by –

$$p_i(s) = R(s)r_i(s) + p(s)$$

The distribution loads due to tendon tension is given by –

$$f_t = -\sum_{i=1}^{n} \tau_i \frac{{p_i}'}{||\dot{p}_i||^3} \ddot{p}_i$$

$$l_t = -\sum_{i=1}^{n} \tau_i (Rr_i) \frac{{p_i}'}{||\dot{p}_i||^3} \ddot{p}_i$$

After expressing the force and moment distributions in kinematic variables, we finally get –

$$\begin{bmatrix} \dot{v} \\ \dot{u} \end{bmatrix} = \begin{bmatrix} K_{se} + A & G \\ B & K_{bt} + H \end{bmatrix}^{-1} \begin{bmatrix} d \\ c \end{bmatrix}$$

III. CONTINUUM ROBOT MODEL

For this study we work with robot with spring steel backbone with acrylic spacer disks and a single Kevlar tendon. To create an experimentally accurate model of tendon robot, the parameters are taken from [31]. The rod parameters were calibrated using weight release trial method. The properties of the steel backbone continuum robot are shown in Table. 1.

TABLE I. TENDON ROBOT PARAMETERS

Properties	Variable	Value
Backbone Length	$\boldsymbol{L\ (m)}$	$\mathbf{0.4}$
Backbone Diameter	r (m)	0.0009
Tendon offset	l (m)	0.019
Mass of system	$g\ (\frac{m}{s^2})$	[9.81 0 0]
Direction of gravity	ρ	39317
Density	$E\ (Pa)$	$207e^9$
Elastic Modulus	$G\ (Pa)$	$7.96e^{10}$
Shear Modulus	$L\ (m)$	0.4

End effector position and orientation are computed for various tendon tension representations by solving static equations using the ode45 solver. The routines are written in MATLAB and solved with the "fsolve" using Levenberg Marquardt solver. Following that, the rotation matrix is transformed to quaternions. Quaternions are versatile and don't have parameterization singularities (gimble lock).

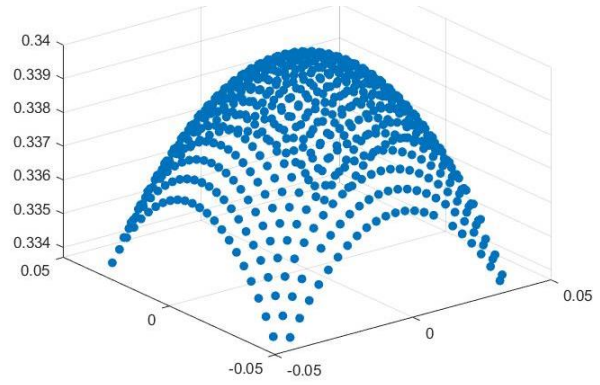

Figure 1. Workspace of the continuum robot

International Journal of Engineering Research & Technology (IJERT)
ISSN: 2278-0181
Vol. 11 Issue 04, April-2022

Quaternions also provide smooth orientation interpolation and efficient rotation composition. The reachable places of the robot end effector are referred to as the robot workspace. The point cloud in Fig. 1 displays the end effector position, which was mapped to configuration space using a 20000 set of randomized tendon tensions.

IV. CASCADE CORRELATION

In artificial neural networks, during the backpropagation step, the weights in the network are changing at once, which leads to the moving target problem. This leads to slow learning as the hidden units observe a constantly changing environment. Cascade correlation algorithm as shown in Fig. 2 was proposed to solve the problem [32].

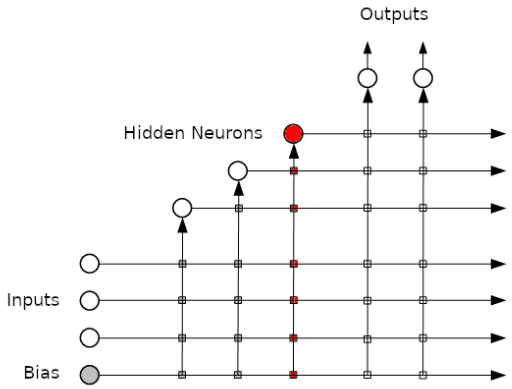

Figure 2. Cascade Network Architecture

Cascade correlation network as shown in Fig starts with the minimal network and then train and add new hidden units automatically. Initially, the input and output are connected with adjustable weights. There is also a bias, which is permanently set to +1. The output of the given configuration is non-linear sum of their weighted inputs.

Following this, hidden units are added one by one. Each hidden unit receives inputs from existing hidden units and origin inputs. Once a unit is added, the input weights are frozen and only the output weights are trained repeatedly. The output weights are trained using the Fahlman's quickprop algorithm. Once the training reaches an asymptote, forward propagation is done one last time to measure the training error. Training stops if we are satisfied with the residual error, if we are not hidden units are added.

To create a new hidden unit, multiple candidate units are evaluated. Each candidate unit is connected to original inputs and existing hidden units. The output of the candidate unit is not connected to the output unit. The weights of the candidate unit are adjusted upon training with the goal to maximise S, S is defined as the sum of sum over all output units o of the magnitude of the correlation (or, more precisely, the covariance) between V, the candidate unit's value, and E_o, the residual output error observed at unit o. S is given by –

$$S = \sum_o \left| \sum_p (V_p - \bar{V})(E_{p,o} - \overline{E_o}) \right|$$

To maximise S, the partial derivate wrt weights is taken and using gradient descent S can be maximised. The candidate unit is chosen whose correlation is the best. The gradient is defined as –

$$\partial S / \partial w_i = \sum_{p,o} \sigma_o (E_{p,o} - \overline{E_o}) f'_p I_{i,p}$$

Where σ_o is the sign of the correlation between the candidate's value and output o, f'_p is the derivative for pattern p of the candidate unit's activation function with respect to the sum of its inputs, and $I_{i,p}$ is the input the candidate unit receives from unit i for pattern p.

Once S stops improving the new candidate is added to the network, the input weights are frozen and the process is continued. As the candidate unit develops a positive correlation with the magnitude of the error, it develops a negative correlation with the weights of the unit, therefore cancelling some of the error. Using a pool of candidates is beneficial as it reduces the chances of installing a useless unit into the network. Since the candidates do not interact with each other and they receive the same input units, training speed can be improved by using parallel machines.

V. RESULTS

To put the model to the test, 20000 random tendon stresses are collected. The network output is used to calculate the end effector location and orientation in quaternions. The dataset is normalized between 0 and 1 to increase model accuracy and speed up the training process. The network has been trained on 97% of the dataset.

Network Performance

Cascade correlation network was trained for 1000 iterations with candidate units selected over 100 iterations. The RMSE error obtained over the training period is shown in Fig. The network was best trained with 10 hidden units and sigmoid function as the activation function. 5 models of the past namely Multi-layer Perceptron, Radial Basis Function, K Nearest Neighbors Regression, Decision Tree, Extreme Learning Machine etc. are modelled to validate the effectiveness and accuracy of our proposed network. The RMSE errors on both training and testing dataset is shown in Table II. Cascade Correlation with sigmoid activation functions is compared against their results and outperforms with significantly lower RMSE values, 1.34 and 1.45, both

TABLE II. RESULTS OF DIFFERENT MODELS

Model	RMSE Training	RMSE Testing	Max Error (mm)
KNNR	1.51	1.87	7.83
RBF	2.83	2.99	6.45
MLP	2.65	2.69	6.25
ELM	1.76	1.84	5.85
Decision Tree	1.17	1.97	11.00
Cascade Correlation	**1.34**	**1.45**	4.13
Cascade Forward backprop	1.68	1.70	5.90

International Journal of Engineering Research & Technology (IJERT)
ISSN: 2278-0181
Vol. 11 Issue 04, April-2022

on train and test data. Figure 3 visually compares the RMSE errors of the literature and proposed models, showing improvement.

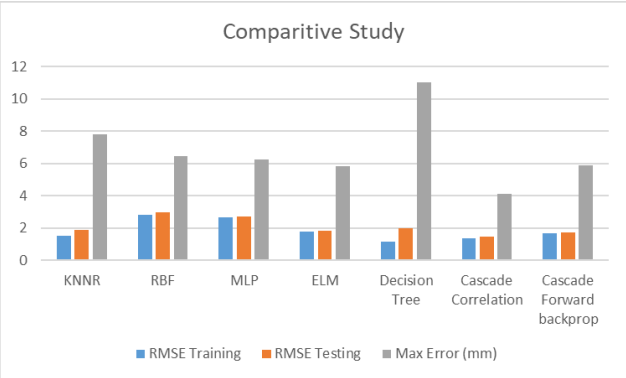

Figure 3. Results of different models compared; Cascade Correlation outperforms other networks

VI. Conclusion

Continuum robot manipulators though complex to control and analyze, offer flexibility and dexterity for a wide array of tasks. In this paper, a static model based on Cosserat model is presented for a single Kevlar tendon. The inverse kinematic of the proposed robot model is obtained through a cascade correlation neural network. Forward kinematic equations are first derived using Cosserat rod model, and datasets containing the robot end-effector in Cartesian space and the tendon tensions are prepared accordingly. The network is then constructed as the IK solver, and the performance is evaluated under different model parameters. From the simulation, a mean squared error of 1.34 can be achieved. The proposed model is then compared to previous literature, validating significant improvement in prediction accuracy.

REFERENCES

[1] Robinson, G., & Davies, J. (1999). Continuum robots - a state of the art. Proceedings 1999 IEEE International Conference on Robotics and Automation

[2] Grzesiak, A., Becker, R., & Verl, A. (2011). The Bionic Handling Assistant: a success story of additive manufacturing. Assembly Automation, 31(4), 329–333.

[3] Hu, H., Wang, P., Zhao, B., Li, M., & Sun, L. (2009). Design of a novel snake-like robotic colonoscope. 2009 IEEE International Conference on Robotics and Biomimetics (ROBIO).

[4] Laschi, C., Mazzolai, B., Mattoli, V., Cianchetti, M., & Dario, P. (2009). Design of a biomimetic robotic octopus arm. Bioinspiration & Biomimetics, 4(1), 015006.

[5] Camarillo, D. B., Krummel, T. M., & Salisbury, J. (2004). Robotic technology in surgery: Past, present, and future. The American Journal of Surgery, 188(4), 2–15.

[6] Tsukagoshi, H., Kitagawa, A., & Segawa, M. (2001). Active Hose: an artificial elephant's nose with maneuverability for rescue operation. Proceedings 2001 ICRA. IEEE International Conference on Robotics and Automation

[7] Godage, I. S., Branson, D. T., Guglielmino, E., & Caldwell, D. G. (2012). Pneumatic muscle actuated continuum arms: Modelling and experimental assessment. 2012 IEEE International Conference on Robotics and Automation.

[8] Webster, R. J., Romano, J. M., & Cowan, N. J. (2009). Mechanics of Precurved-Tube Continuum Robots. IEEE Transactions on Robotics, 25(1), 67–78.

[9] Seok, S., Onal, C. D., Cho, K. J., Wood, R. J., Rus, D., & Kim, S. (2013). Meshworm: A Peristaltic Soft Robot with Antagonistic Nickel Titanium Coil Actuators. IEEE/ASME Transactions on Mechatronics, 18(5), 1485–1497.

[10] Camarillo, D., Carlson, C., & Salisbury, J. (2009). Configuration Tracking for Continuum Manipulators with Coupled Tendon Drive. IEEE Transactions on Robotics, 25(4), 798–808.

[11] Hannan, M. W., & Walker, I. D. (2001). Analysis and experiments with an elephant's trunk robot. Advanced Robotics, 15(8), 847–858.

[12] Dermatas, E., Nearchou, A., & Aspragathost, N. (1996). Error-back-propagation solution to the inverse kinematic problem of redundant manipulators. Robotics and Computer-Integrated Manufacturing, 12(4), 303–310.

[13] Rone, W. S., & Ben-Tzvi, P. (2014). Continuum Robot Dynamics Utilizing the Principle of Virtual Power. IEEE Transactions on Robotics, 30(1), 275–287.

[14] Jones, B., & Walker, I. (2006). Kinematics for multisection continuum robots. IEEE Transactions on Robotics, 22(1), 43–55.

[15] He, B., Wang, Z., Li, Q., Xie, H., & Shen, R. (2013). An Analytic Method for the Kinematics and Dynamics of a Multiple-Backbone Continuum Robot. International Journal of Advanced Robotic Systems, 10(1), 84.

[16] Li, M., Kang, R., Geng, S., & Guglielmino, E. (2017). Design and control of a tendon-driven continuum robot. Transactions of the Institute of Measurement and Control, 40(11), 3263–3272.

[17] Jones, B. A., Gray, R. L., & Turlapati, K. (2009). Three dimensional statics for continuum robotics. 2009 IEEE/RSJ International Conference on Intelligent Robots and Systems.

[18] Rucker, D. C., & Webster III, R. J. (2011). Statics and Dynamics of Continuum Robots with General Tendon Routing and External Loading. IEEE Transactions on Robotics, 27(6), 1033–1044.

[19] Song, S., Li, Z., Yu, H., & Ren, H. (2015). Shape reconstruction for wire-driven flexible robots based on Bézier curve and electromagnetic positioning. Mechatronics, 29, 28–35.

[20] Ding, J., Goldman, R. E., Xu, K., Allen, P. K., Fowler, D. L., & Simaan, N. (2013). Design and Coordination Kinematics of an Insertable Robotic Effectors Platform for Single-Port Access Surgery. IEEE/ASME Transactions on Mechatronics, 18(5), 1612–1624.

[21] Kuntz, A., Sethi, A., Webster, R. J., & Alterovitz, R. (2020). Learning the Complete Shape of Concentric Tube Robots. IEEE Transactions on Medical Robotics and Bionics, 2(2), 140–147.

[22] Loutfi, I. M., Boutchouang, A. B., Melingui, A., Lakhal, O., Motto, F. B., & Merzouki, R. (2020). Learning-Based Approaches for Forward Kinematic Modeling of Continuum Manipulators. IFAC-PapersOnLine, 53(2), 9899–9904.

[23] Shahabi, E., & Kuo, C. H. (2018). Solving Inverse Kinematics of a Planar Dual-Backbone Continuum Robot Using Neural Network. EuCoMeS 2018, 355–361.

[24] Wu, G., Shi, G., & Shi, Y. (2017). Modeling and analysis of a parallel continuum robot using artificial neural network. 2017 IEEE International Conference on Mechatronics (ICM).

[25] Lai, J., Huang, K., & Chu, H. K. (2019). A Learning-based Inverse Kinematics Solver for a Multi-Segment Continuum Robot in Robot-Independent Mapping. 2019 IEEE International Conference on Robotics and Biomimetics (ROBIO).

[26] Shen, W., Yang, G., Zheng, T., Wang, Y., Yang, K., & Fang, Z. (2020). An Accuracy Enhancement Method for a Cable-Driven Continuum Robot with a Flexible Backbone. IEEE Access, 8, 37474–37481.

[27] Xu, W., Chen, J., Lau, H. Y., & Ren, H. (2016). Data-driven methods towards learning the highly nonlinear inverse kinematics of tendon-driven surgical manipulators. The International Journal of Medical Robotics and Computer Assisted Surgery, 13(3)

[28] Thuruthel, T. G., Falotico, E., Cianchetti, M., & Laschi, C. (2016). Learning Global Inverse Kinematics Solutions for a Continuum Robot. ROMANSY 21 - Robot Design, Dynamics and Control, 47–54.

[29] Rucker, D. C., & Webster III, R. J. (2011). Statics and Dynamics of Continuum Robots With General Tendon Routing and External Loading. *IEEE Transactions on Robotics*, *27*(6), 1033–1044.

[30] Jones, B. A., Gray, R. L., & Turlapati, K. (2009). Three dimensional statics for continuum robotics. *2009 IEEE/RSJ International Conference on Intelligent Robots and Systems*.

[31] Till, J., Aloi, V., & Rucker, C. (2019). Real-time dynamics of soft and continuum robots based on Cosserat rod models. The International Journal of Robotics Research, 38(6), 723–746.

[32] Liang, H. (1998). Improvement of cascade correlation learning. *Information Sciences*, *112*(1–4), 1–6.